Geophys. J. Int. (2010) **180,** 635–650 doi: 10.1111/j.1365-246X.2009.04437.x

Gravity variations induced by core flows

Mathieu Dumberry

Department of Physics, University of Alberta, Edmonton, Canada T6G 2G7. *E-mail: dumberry@phys.ualberta.ca*

Accepted 2009 October 29. Received 2009 October 29; in original form 2009 May 22

SUMMARY

The temporal variation in the density structure associated with convective motions in the outer core causes a change in the Earth's gravity field. Core flows also lead to a gravity change through the global elastic deformations that accompany changes in the non-hydrostatic pressure at the core–mantle boundary (CMB). In this work, we present predictions of the gravity changes from these two processes during the past century. These predictions are built on the basis of flows at the surface of the core that are reconstructed from the observed geomagnetic secular variation. The pressure-induced gravity variations can be reconstructed directly from surface core flows under the assumption of tangential geostrophy; predicted variations in the Stokes coefficients of degree 2, 3 and 4 are of the order of 10^{-11}, 3×10^{-12} and 10^{-12}, respectively, with a typical timescale of a few decades. These correspond to changes in gravity of 70, 30 and 15 nGal, and to equivalent geoid height variations of 0.15, 0.05 and 0.02 mm, respectively. The density-induced gravity variations cannot be determined solely from surface core flows, though a partial recovery is possible if flows with important axial gradients dominate the dynamics at decadal timescales. If this is the case, the density-induced gravity signal is of similar amplitude and generally anti-correlated with the pressure-induced signal, thus reducing the overall amplitude of the gravity changes. However, because we expect decadal flows to be predominantly axially invariant, the amplitude of the density-induced gravity changes should be much smaller. Our prediction also allows to determine upper bounds in pressure change at the CMB and density change within the core that have taken place during the past 20 yr such that observed gravity variations are not exceeded; for harmonic degree 2, we find a maximum pressure change of approximately 350 Pa and a maximum departure from hydrostatic density of approximately 1 part in 10^7. Although the predicted gravity changes from core flows are small, they are at the threshold of detectability with high-precision gravity measurements from satellite missions such as GRACE. The most important challenge to identifying a core signal will be the removal of interannual gravity variations caused by surface processes which are an order of magnitude larger and mask the core signal.

Key words: Gravity anomalies and Earth structure; Time variable gravity; Dynamo: theories and simulations; Core, outer core and inner core.

1 INTRODUCTION

Gravity variations recorded at the Earth's surface occur over a wide range of timescales. At a diurnal timescale, tidal interactions with the Moon, the Sun and other planets are responsible for the observed variations (e.g. Agnew 2007). At a timescale of a few years and shorter, the variations are dominantly caused by mass displacements induced by ocean currents and atmospheric circulation, as well as those occurring in the cryosphere and hydrosphere (e.g. Chen & Wilson 2003). Gravity variations occurring over a timescale of thousands of years are caused by postglacial rebound (e.g. Tamisiea *et al.* 2007). On a much longer timescale of millions of years, sufficiently long that over the accessible time span of observation the gravity signal appears static, the largest variations are from mass displacements involved in mantle convection (e.g Hager *et al.* 1985).

Observations indicate that gravity variations also occur over interannual and decadal timescales (e.g. Cox & Chao 2002; Chen & Wilson 2003). Some of these observed changes are undoubtedly the result of surface processes. However, it is possible that decadal variations may comprise a part induced by fluid motion in the outer core. Indeed, inversions of geomagnetic secular variation reveal the presence of core flows that vary on a timescale of decades (Bloxham & Jackson 1991; Holme 2007). Should these flows have the ability to generate density variations, decadal gravity variations from these can be expected.

The most straightforward way by which core flows create density variations is simply through the displacement in time of density heterogeneities within the core that they induce. The latter are either directly entrained by core flows or related to them through an evolving force balance. Displaced mass in the core results in a global

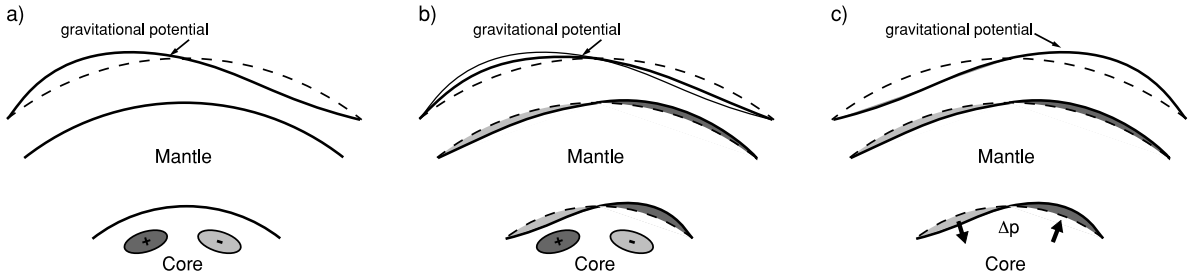

Figure 1. Gravitational potential variations at the surface caused by time-dependent core flows. In all three figures, the deflection of the surface of constant gravitational potential is depicted by the warped thick solid curve above the Earth's surface (the unperturbed gravitational potential is represented by the dashed line). Similarly, deflections of the CMB and Earth's surface are shown as warped solid lines (dashed lines represent their unperturbed geometry). Dark and light grey areas represent positive and negative density changes, respectively. (a) Gravitational potential variations from density perturbations in the core. Positive density anomalies ('+') produce an upward deflection and negative anomalies ('−') lead to a downward deflection. (b) The density variations induced by global elastic deformations contribute to an additional perturbation in gravity. Shown on the figure are the density perturbations resulting from the deflection of the CMB and the Earth's external surface. The deflection of density surfaces within the mantle and core also contribute to the density perturbations but are not shown. The total gravitational potential at the surface (thick solid line) is the sum of that from the imposed density change in the core (thin solid line) and that from the associated global elastic deformations. We note that the sign and amplitude of the surface deflections and potential change shown on the figure are for the purpose of illustration only; they are non-trivial functions of the radial profiles of hydrostatic density and elastic moduli as well as on the wavelength and depth of the density perturbation within the core. (c) Gravitational potential variations resulting from horizontal pressure gradients at the CMB. The change in the normal surface force on the CMB, shown by the black arrows, perturbs the mechanical equilibrium and lead to global elastic deformations which includes deflection of the CMB and the Earth's surface (shown on the figure) as well as deflections of the density surfaces within the mantle and core (not shown). The potential change at the surface results from the integrated density perturbation of these elastic displacements.

change in gravity, including at the Earth's surface (Fig. 1a). This perturbation of the internal gravity field must be accompanied by global elastic deformations, taking place in order to maintain the mechanical equilibrium of the planet. These entrain a secondary density perturbation, also contributing to the change in gravity (Fig. 1b).

Core flows also lead to density variations through their interaction with the inner core and mantle. First, a change in core flows involves a change in the non-hydrostatic pressure inside the core. This entrains a change in the normal surface force acting on the core–mantle boundary (CMB), thereby altering the mechanical equilibrium, leading to global elastic deformations and, consequently, to changes in gravity (Fig. 1c, e.g. Merriam 1988). The same process occurs at the inner core boundary (ICB). Second, flows near the CMB and ICB can lead to torques on the mantle and inner core. Subject to a torque, the inner core will undergo a differential rotation with respect to the mantle. Because the inner core density structure is not spherically symmetric, this entrains gravity variations as viewed in the mantle frame. This is the case for an equatorial rotation of the elliptical geometric figure of the inner core (Dumberry 2008), and also for an axial rotation of the inner core if its density is not axially symmetric (e.g Mound & Buffett 2003). Additionally, the change in mantle rotation imposed by the requirement of angular momentum conservation through these torques lead, by mechanical deformation, to a secondary change in its moment of inertia, and thus to a change in gravity.

The focus of the present study is on gravity variations induced by time-dependent density heterogeneities within the fluid core as well as those caused by changes in pressure at the CMB. Our goal is to attempt a recovery of these variations on the basis of temporal variations in core flows near the CMB that are themselves reconstructed from the observed geomagnetic secular variation.

The prospect of recovering the pressure-induced gravity variations is better than that for the density-induced part. This is because if one assumes that the horizontal force balance near the surface of the core is tangentially geostrophic (Hills 1979; Le Mouël 1984), horizontal pressure gradients are directly related to core flows. The axially symmetric component of gravity changes inferred from this method have already been investigated by Fang *et al.* (1996), Dumberry & Bloxham (2004) and Greff-Lefftz *et al.* (2004). Here, we extend this investigation to also include non-axisymmetric gravity variations.

The gravity signal caused by decadal changes in density heterogeneities within the core is more difficult to constrain from observations. First, this is because we require knowledge of density heterogeneities not only near the CMB but also deeper in the core. To infer the latter from surface core flows requires additional dynamic assumptions which may not be valid. Second, and more importantly, the recovery of density heterogeneities depends on the radial shear of the flow near the CMB. This part of the core flow cannot be constrained robustly with geomagnetic observations (Jault & Le Mouël 1991; Whaler & Davis 1997). Thus, we expect the density-induced gravity variations to be less reliably determined than the pressure-induced part.

Gravity variations from these processes are expected to be small. For instance, variations in the elliptical component of the gravity field, J_2, caused by pressure changes at the CMB are expected to be on the order of 10^{-11} (Dumberry & Bloxham 2004; Greff-Lefftz *et al.* 2004). This corresponds to a change of approximately 150 nGal at the surface, or a corresponding change in geoid height of 0.3 mm, and is an order of magnitude smaller than some of the observed variations (Cox & Chao 2002; Chao *et al.* 2003). As for the density-induced gravity, given that departures in density from the hydrostatic reference state are expected to be of the order of one part in 10^9 (Stevenson 1987), one may be tempted to neglect this contribution entirely. However, as shown in the study of Jiang *et al.* (2007), and as we will show in the present study, despite their small size, they can lead to gravity variations of the same order as those from pressure.

Although small, variations at the longest wavelength from core processes are larger than the accuracy of superconducting gravimeters (Hinderer *et al.* 2007) and of the same order as that of the GRACE satellite mission (Tapley *et al.* 2004). With the anticipation of future improvements in gravity observations, it may eventually become possible to recover a gravity signal from the core. Since this

gravity signal is connected to core flows, it would open the prospect of using gravity observations to confirm or further constrain core flows inverted from geomagnetic observations.

The main objective of our study is to build a prediction of the gravity changes induced by core flows. This requires first to establish the theoretical framework appropriate to do so; this is done in Section 2. Predictions based on this theory and on time-dependent models of core surface flows are presented in Sections 3 and 4. In Section 3, we investigate the gravity variations in the time interval 1900–1990. This allows to determine the amplitude of the decadal gravity variations that result from core flows. In Section 4, we focus on the more recent time interval of 1985–2005, where we can also compare our predictions with actual observations of gravity variations. The prospect of detecting core-flow induced gravity variations and the conditions required to do so can then be assessed. The observed gravity variations also allow to establish tentative bounds on pressure and density changes within the core that have occurred in the past two decades. This is an important issue in the light of a recent suggestion that time-dependent heterogeneities in the core can be inferred seismically (Dai & Song 2008). If one wants to invoke density heterogeneities as a preferred explanation for these seismic anomalies, one must make sure that the predicted gravity signal from these do not exceed the observed signal. Finally, in Section 5, we conclude with a summary and a discussion of our results.

2 THEORY

2.1 Gravity variations

As shown in Fig. 1(a), density perturbations ρ' with respect to the background hydrostatic density ρ_o in the core result in a change in gravitational potential everywhere inside the Earth. This potential, which we denote by V_1, perturbs the internal force balance and small elastic deformations take place in order to maintain the global mechanical equilibrium. The global density change that results from the latter produces an additional contribution to the gravitational potential, as depicted in Fig. 1(b), which we denote by V_2.

Changes in the horizontal gradient of the non-hydrostatic pressure field p at the CMB result in a change in the normal force applied on the CMB. This perturbs the mechanical equilibrium and consequently, global elastic deformations must take place. These deformations cause a change in the gravitational potential (Fig. 1c) and we denote this contribution to the potential by V_3.

The density heterogeneities ρ' and the non-hydrostatic pressure p in the core are both associated with core flows. Temporal variations in these flows lead to changes in ρ' and p and thus to temporal variations in the gravitational potential $V = V_1 + V_2 + V_3$. Our aim is to build a prediction of V at the surface of the Earth based on time-dependent variations ρ' and p in the core.

Let us write the gravitational potential at the surface (radius $r = r_e$) as an expansion of surface spherical harmonics,

$$V(r_e) = \sum_{l=2}^{\infty}\sum_{m=0}^{l}\left[{}_c\phi_l^m \cos m\phi + {}_s\phi_l^m \sin m\phi\right] P_l^m(\cos\theta)\,, \tag{1}$$

where (r, θ, ϕ) are spherical polar coordinates and $P_l^m(\cos\theta)$ are associated Legendre polynomials. Given a model of ρ' within the core and p at the CMB, expanded, respectively, as

$$\rho'(r) = \sum_{l=2}^{\infty}\sum_{m=0}^{l}\left[{}_c\rho_l^m(r)\,\cos m\phi + {}_s\rho_l^m(r)\,\sin m\phi\right] P_l^m(\cos\theta)\,, \tag{2}$$

$$p = \sum_{l=2}^{\infty}\sum_{m=0}^{l}\left[{}_c\Psi_l^m \cos m\phi + {}_s\Psi_l^m \sin m\phi\right] P_l^m(\cos\theta)\,, \tag{3}$$

our task is to determine the coefficients ${}_c\phi_l^m$ and ${}_s\phi_l^m$ of the gravitational potential in terms of the coefficients ${}_c\,\rho_l^m(r)$, ${}_s\,\rho_l^m(r)$, ${}_c\Psi_l^m$ and ${}_s\Psi_l^m$. Note that in (1), (2) and (3), the summation does not include terms with $l = 0$ and 1; we assume in this study that mass is conserved and that core motions do not change the location of the centre of mass. [Degree-one perturbations in gravity are considered in the study of Greff-Lefftz & Legros (2007).]

We further specify that the associated Legendre polynomials are normalized such that

$$\int \left[P_l^m \cos m\phi\right]^2 \mathrm{d}\Omega = \int \left[P_l^m \sin m\phi\right]^2 \mathrm{d}\Omega = \frac{4\pi}{2l+1}\,. \tag{4}$$

Using this so-called Gauss–Schmidt normalization is convenient because it follows the usual convention employed in geomagnetism. This choice will facilitate the relationship between coefficients of density and pressure with those of core flows that are retrieved from the geomagnetic secular variation.

In geodesy, the usual convention is different: the associated Legendre polynomials are normalized such that the right-hand side of (4) is equal to 4π. The gravitational potential $V(r)$ at a radius r above the Earth's surface is commonly reported in terms of the following spherical harmonic expansion,

$$V(r) = -\frac{GM}{r}\left[1 + \sum_{l=2}^{\infty}\sum_{m=0}^{l}\left(\frac{r_e}{r}\right)^l \mathcal{V}_{lm}\right], \tag{5}$$

where M is the mass of the Earth and

$$\mathcal{V}_{lm} = (C_{lm}\cos m\phi + S_{lm}\sin m\phi)\,\bar{P}_l^m(\cos\theta)\,. \tag{6}$$

The coefficients C_{lm} and S_{lm} are known as Stokes coefficients, and $\bar{P}_l^m(\cos\theta)$ are related to our Gauss–Schmidt normalized $P_l^m(\cos\theta)$ by $\bar{P}_l^m(\cos\theta) = \sqrt{2l+1}\,P_l^m(\cos\theta)$.

For convenience, we will use the expansion of the potential given by eq. (1) in the development of the next two subsections. Ultimately, it will be necessary to transform the predicted changes in the coefficients ${}_c\phi_l^m$ and ${}_s\phi_l^m$ into changes in terms of Stokes coefficients C_{lm} and S_{lm}.

2.1.1 Gravity changes from density heterogeneities in the core

Let us suppose a density perturbation in the core concentrated in a thin radial surface of thickness dr at radius r and expressed in terms of a surface mass density $\sigma(r)$. We expand $\sigma(r)$ in terms of a spherical harmonic decomposition as in (1) with coefficients $\sigma_\alpha(r)$. Here, we have introduced a short-hand notation, where we write $\sigma_\alpha(r)$ to represent a single spherical harmonic coefficient with a specific combination of l and m and subscript c or s. The surface mass density causes a change in the gravitational potential V_1 at the Earth's surface and the coefficients of these two quantities are related by (e.g. Kaula 1968)

$$\phi_\alpha^{(1)} = -\frac{4\pi G}{2l+1}\frac{r^{l+2}}{r_e^{l+1}}\sigma_\alpha(r), \tag{7}$$

where G is the gravitational constant. Fig. 2 shows how $\phi_\alpha^{(1)}$ changes as a function of the radius at which the surface mass density is applied for harmonic degrees $l = 2$– 6. In these calculations, the amplitude of the surface mass density coefficients is constant and chosen such that $\phi_\alpha^{(1)} = 1$ at the CMB for $l = 2$. Fig. 2 illustrates how density perturbations with long wavelength and near the CMB

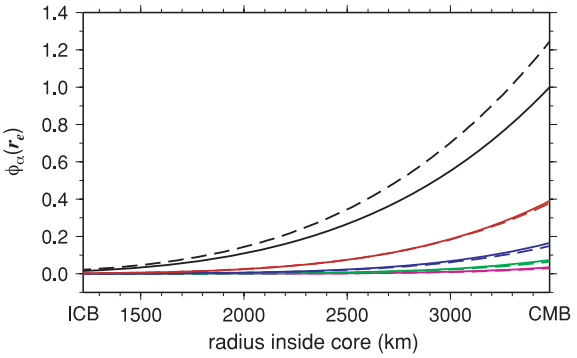

Figure 2. Amplitude of the gravitational potential at the Earth's surface as a function of the radius at which a surface mass density is applied within the outer core for spherical harmonic degree $l = 2$ (black), $l = 3$ (red), $l = 4$ (blue), $l = 5$ (green) and $l = 6$ (purple). Solid lines show the potential for a rigid Earth (no elastic deformations, $\phi_\alpha^{(1)}$ as given by eq. 7). Dashed lines show the potential when the contribution from elastic deformations is included ($\phi_\alpha^{(1)} + \phi_\alpha^{(2)}$). The amplitude of the applied surface mass density is constant, with an amplitude chosen such that $\phi_\alpha^{(1)} = 1$ at the CMB for $l = 2$.

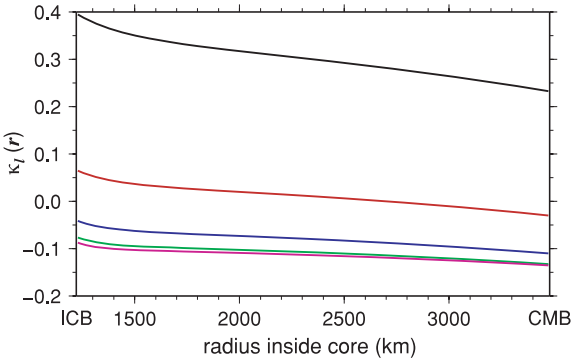

Figure 3. The contribution to the gravitational potential at the surface of the Earth caused by elastic deformations, $\kappa_l(r)$, as a function of the radius in the fluid core at which the surface mass density is applied, for spherical harmonic degree $l = 2$ (black), $l = 3$ (red), $l = 4$ (blue), $l = 5$ (green) and $l = 6$ (purple).

lead to a comparatively larger change in gravitational potential than density perturbations with shorter wavelength or seated deeper in the core.

To the potential V_1, we must add the contribution from elastic deformations V_2 with coefficients $\phi_\alpha^{(2)}$. For small density perturbations in the core, the density variations from elastic deformations are also small and the coefficients $\phi_\alpha^{(2)}$ are linearly related to the coefficients $\phi_\alpha^{(1)}$ through

$$\phi_\alpha^{(2)} = \kappa_l(r)\, \phi_\alpha^{(1)} . \tag{8}$$

The factor $\kappa_l(r)$ characterizes the response of the Earth to an applied internal load. Its numerical value represents the relative importance of $\phi_\alpha^{(2)}$ compared to that of $\phi_\alpha^{(1)}$ for a surface mass density of harmonic degree l located at radius r within the core. Note that it does not depend on spherical order m. In Fig. 3, we show how $\kappa_l(r)$ varies as a function of the radius r at which the surface mass density is applied and for $l = 2$– 6. These values have been calculated in a manner similar to that detailed in Dumberry & Bloxham (2004) but adapted for the present problem; a brief summary of this method is given in the Appendix. For $l = 2$, elastic deformations increase the amplitude of the gravitational potential at the surface by approximately 30 per cent. For $l > 2$, elastic deformations contribute to a change of approximately 10 per cent or less compared to a rigid Earth. We note that $\kappa_l(r)$ can be both positive or negative: whether elastic deformations contribute to an increase or decrease in the resulting potential at the surface is a complex function of the radial profile of the hydrostatic density and elastic parameters and depends also on the harmonic degree and location of the imposed density perturbation. A case in point is $\kappa_3(r)$, which is positive when the density perturbation is deep in the core, but negative when it is close to the CMB.

For a given coefficient of surface mass density, the combined change in the gravitational potential is the sum of (7) and (8)

$$\phi_\alpha = \phi_\alpha^{(1)}\, [1 + \kappa_l(r)] . \tag{9}$$

We show in Fig. 2 how the gravitational potential at the Earth's surface is changed by the inclusion of the contribution from elastic deformations (dashed lines). While elastic deformations modify the gravitational potential significantly for $l = 2$, their effect are less important for $l > 2$.

For a general density distribution, the change in gravitational potential at the Earth's surface is then obtained by an integration over the thickness of the fluid core,

$$\phi_\alpha = -\frac{4\pi G}{2l+1} \frac{1}{r_e^{l+1}} \int_{r_i}^{r_f} \rho_\alpha(r)\, [1 + \kappa_l(r)]\, r^{l+2}\, \mathrm{d}r , \tag{10}$$

where $\sigma_\alpha(r) = \rho_\alpha(r)\mathrm{d}r$ and r_i and r_f are the radii of the inner core and fluid core, respectively.

The strategy that we have employed to take into account the elastic response of the Earth to applied internal loads is equivalent to that used to explain the static part of the gravitational potential in terms of mantle density heterogeneities (e.g. Richards & Hager 1984; Defraigne *et al.* 1996). The difference here is that our load numbers are calculated for density perturbations taking place within the core as opposed to within the mantle.

In terms of changes in Stokes coefficients, density variations expressed by the coefficients defined in (2) lead to the following changes in ΔC_{lm} and ΔS_{lm},

$$\Delta C_{lm} = \frac{4\pi}{(2l+1)^{3/2}} \frac{1}{M r_e^l} \int_{r_i}^{r_f} {}_c\rho_l^m(r)\, [1 + \kappa_l(r)]\, r^{l+2}\, \mathrm{d}r , \tag{11}$$

$$\Delta S_{lm} = \frac{4\pi}{(2l+1)^{3/2}} \frac{1}{M r_e^l} \int_{r_i}^{r_f} {}_s\rho_l^m(r)\, [1 + \kappa_l(r)]\, r^{l+2}\, \mathrm{d}r . \tag{12}$$

Thus, ΔC_{lm}, ΔS_{lm} vary as $(r_f/r_e)^l(2l+1)^{-3/2} \approx 2^{-l}(2l+1)^{-3/2}$ with harmonic degree l; a density change in the core of the same amplitude but higher degree results in smaller gravity variation at the surface.

2.1.2 Gravity changes from pressure variations at the CMB

A change in non-hydrostatic pressure at the CMB perturbs the mechanical equilibrium. The induced global elastic deformations lead to global density variations and to an associated change in gravitational potential. To determine the gravitational potential at the Earth's surface that results from a given change in pressure at the CMB, it is necessary to solve the set of elastic-gravitational equations for small displacements in the whole Earth. Details of how this is done can be found in Dumberry & Bloxham (2004) and Greff-Lefftz *et al.* (2004). Given a pressure field at the CMB expanded

Table 1. Parameters used in calculations.

Parameter	Value
Gravitational constant	$G = 6.67 \times 10^{-11}$ m^3 kg^{-1} s^{-2}
Mass of the Earth	$M = 5.97 \times 10^{24}$ kg
Radius of Earth	$r_e = 6.371 \times 10^6$ m
Radius of the core	$r_f = 3.480 \times 10^6$ m
Mean density	$\bar{\rho} = 5515$ kg m^{-3}
Density of core at CMB	$\rho_f = 9\,903$ kg m^{-3}
Gravitational acceleration at CMB	$g_f = 10.682$ m s^{-2}
Rotation frequency	$\Omega = 7.292 \times 10^{-5}$ s^{-1}
Elastic coefficients	$\bar{k}_2 = 1.116 \times 10^{-1}$
	$\bar{k}_3 = 3.304 \times 10^{-2}$
	$\bar{k}_4 = 1.156 \times 10^{-2}$
	$\bar{k}_5 = 4.560 \times 10^{-3}$
	$\bar{k}_6 = 1.957 \times 10^{-3}$

in spherical harmonics with coefficients Ψ_α, the change in gravitational potential at the surface can be expressed in a concise manner as

$$\phi_\alpha^{(3)} = -\frac{\bar{k}_l \Psi_\alpha}{\bar{\rho}}\,, \tag{13}$$

where $\bar{\rho}$ is the mean density of the Earth. The coefficients $\bar{k}_l$ allow to relate a pressure change of degree l at the CMB to the change in gravitational potential of the same degree at the surface. Their numerical values have been computed by Dumberry & Bloxham (2004) and Greff-Lefftz *et al.* (2004) and are listed in Table 1.

The change in the Stokes coefficients are then related to the pressure coefficients given in (3) by

$$\Delta C_{lm} = \frac{\bar{k}_l}{\sqrt{2l+1}} \frac{r_e}{GM\bar{\rho}}\, {}_c\Psi_l^m\,, \tag{14}$$

$$\Delta S_{lm} = \frac{\bar{k}_l}{\sqrt{2l+1}} \frac{r_e}{GM\bar{\rho}}\, {}_s\Psi_l^m\,. \tag{15}$$

Thus, ΔC_{lm}, ΔS_{lm} vary as $k_l(2l+1)^{-1/2} \approx 3^{-l}(2l+1)^{-1/2}$ with harmonic degree l; as for the density-induced gravity, a change in pressure at the CMB of the same amplitude but higher harmonic degree results in a smaller gravity change at the Earth's surface.

2.2 Core dynamics

Knowledge of the temporal variations in density in the core and pressure at the CMB allow a prediction of gravity variations at the surface from (11)–(12) and (14)–(15). Changes in both the density and pressure are related to core flows. Our goal is to recover these changes based on flows at the surface of the core, the part that can be retrieved from the geomagnetic secular variation. This is the task on which we concentrate in this section. To do so, an excursion into core dynamics is necessary.

2.2.1 Geostrophic pressure at the CMB

The pressure at the CMB can be related to fluid motions $\mathbf{u}$ on the basis of the Navier–Stokes equation, which in its Boussinesq form is (e.g. Gubbins & Roberts 1987)

$$\rho_o \left(\frac{\partial \mathbf{u}}{\partial t} + \mathbf{u}\cdot\boldsymbol{\nabla}\mathbf{u} + 2\boldsymbol{\Omega}\times\mathbf{u} \right) = -\boldsymbol{\nabla} p + \mathbf{J}\times\mathbf{B} - \rho' g_o \hat{\mathbf{r}} + \rho_o \nu \nabla^2 \mathbf{u}\,, \tag{16}$$

where t is time, $\mathbf{B}$ is the magnetic field, $\mathbf{J}$ is the current density, g_o is the scalar gravitational acceleration, ν is the kinematic viscosity and $\boldsymbol{\Omega} = \Omega\hat{\mathbf{z}}$ is the Earth's rotation vector pointing in the axial direction $\hat{\mathbf{z}}$. In writing (16), we have assumed the flow to be incompressible, an approximation that applies for the whole of this study.

An order of magnitude analysis suggests that inertial and viscous forces are small compared to other terms, leaving a so-called magneto-geostrophic balance between the Coriolis acceleration, pressure gradients, the Lorentz force and buoyancy (e.g. Gubbins & Roberts 1987),

$$2\rho_o \boldsymbol{\Omega}\times\mathbf{u} = -\boldsymbol{\nabla} p + \mathbf{J}\times\mathbf{B} - \rho' g_o \hat{\mathbf{r}}\,. \tag{17}$$

Based on the amplitude of the observed magnetic field at the Earth's surface downward continued to the CMB, the Lorentz force near the surface of the core is expected to be small (e.g. Bloxham & Jackson 1991; Jault & Le Mouël 1991). If this assumption is correct, the flow in the outermost part of the core (in the free stream, outside the thin viscous boundary layer adjacent to the CMB) should then be governed by

$$2\rho_f \Omega\,\hat{\mathbf{z}}\times\mathbf{u} = -\boldsymbol{\nabla} p - \rho' g_f \hat{\mathbf{r}}\,, \tag{18}$$

where ρ_f is the hydrostatic density on the core-side of the CMB and g_f is the gravitational acceleration at the CMB. Taking $\hat{\mathbf{r}}\times$ (18), with $u_r = 0$, we obtain (Le Mouël 1984)

$$2\Omega\rho_f \cos\theta\, \mathbf{u}_\mathrm{h} = \hat{\mathbf{r}}\times\boldsymbol{\nabla}_h p\,, \tag{19}$$

relating horizontal flows $\mathbf{u}_\mathrm{h} = \mathbf{u}_\mathrm{h}(\theta,\phi)$ to horizontal pressure gradients, where $\boldsymbol{\nabla}_h = \boldsymbol{\nabla} - \hat{\mathbf{r}}\frac{\partial}{\partial r}$.

Condition (19) is known as tangential geostrophy. On the basis of this condition, the coefficients of pressure at the CMB, as defined in (3), can be related directly to core flow coefficients and closed form relationships between them are presented in Gire & Le Mouël (1990). By using (14) and (15), a prediction of temporal gravity variations induced by pressure changes at the CMB can be obtained directly from a time-dependent model of core flows.

The amplitude of the gravity changes at the surface of the Earth caused by this process can be determined based on a simple order of magnitude calculation. From (19), a typical change in pressure at the CMB is related to a typical change in the amplitude of core flows $\mathcal{U}$ by,

$$p \sim 2\Omega\rho_f r_f \mathcal{U}\,. \tag{20}$$

Assuming $\mathcal{U} = 1$ km yr^{-1} ($\sim$0.03 mm s^{-1}), typical of changes over a decade inferred from geomagnetic secular variation, and using the parameter values listed in Table 1, we expect pressure variations of the order of 150 Pa. From (14) and (15), such a pressure change at degree 2, 3 and 4 would lead to changes in Stokes coefficients of 2.2×10^{-11}, 5.6×10^{-12} and 1.6×10^{-12}, respectively, consistent with the findings of Dumberry & Bloxham (2004) and Greff-Lefftz *et al.* (2004). These estimates also give a sense of the trend of the gravity change as a function of harmonic degree, decreasing by approximately an order of magnitude for an increase of two in harmonic degree.

2.2.2 Lateral density heterogeneities in the core inferred from a thermal wind balance

A diagnostic equation relating density heterogeneities to core flows can be obtained by taking $\boldsymbol{\nabla}\times$ (17), which gives

$$-2\Omega\rho_o \hat{\mathbf{z}}\cdot\boldsymbol{\nabla}\mathbf{u} = g_o \hat{\mathbf{r}}\times\boldsymbol{\nabla}_h\rho' + \boldsymbol{\nabla}\times(\mathbf{J}\times\mathbf{B})\,. \tag{21}$$

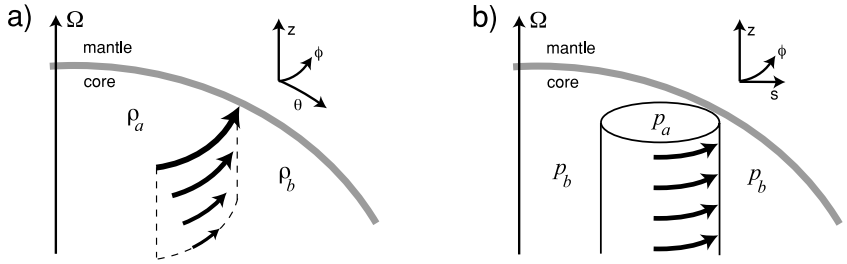

Figure 4. (a) Illustration of a thermal wind flow for the specific case of a density gradient ($\rho_a > \rho_b$) in the latitudinal direction. This density gradient supports an azimuthal flow (black arrows) with a gradient in z, as prescribed by eq. (22). (b) Illustration of a geostrophic flow or the leading order $s-\phi$ component of a quasi-geostrophic flow. The cylindrical outline represents closed contours of the axially invariant flow (black arrows) in the $s-\phi$ direction. This flow is supported by an axially invariant pressure gradient in the $s-\phi$ direction ($p_a < p_b$) as prescribed by eq. (26). In both figures, $\mathbf{\Omega}$ is the Earth's rotation vector and the thick grey line represents the CMB.

The left-hand side of (21) only involves gradients in the flow along the rotation axis, which we refer to as non-rigid flows. In a magneto-geostrophic balance, non-rigid flows can result either from lateral variations in density or from the Lorentz force. If the Lorentz force near the surface of the core is small, as we approximated in the previous section, and with $u_r \approx 0$, then we recover a thermal wind balance

$$-\frac{2\Omega\rho_f}{g_f}\hat{\mathbf{z}}\cdot\nabla\mathbf{u_h} = \hat{\mathbf{r}}\times\nabla_h\rho' \,. \tag{22}$$

An illustration of a thermal wind flow is shown in Fig. 4(a).

Based on (22), lateral density variations near the CMB can be reconstructed from horizontal flows and their axial gradients (e.g. Hulot *et al.* 1990; Jackson & Bloxham 1991). Indeed, eq. (22) has been used to connect the steady part of core flows to lateral temperature variations in the lower mantle (Bloxham & Jackson 1990; Kohler & Stevenson 1990; Amit & Olson 2006). In this scenario, it is assumed that the pattern of lateral density variations in the core is imposed by lateral temperature gradients at the base of the mantle. The amplitude of ρ' is linearly related to lower mantle temperature by a proportionality constant and decays with depth inside the core.

For our present purpose, we are not interested in the steady part of the thermal wind balance but in its decadal variation. In this 'thermal wind' scenario, decadal changes in non-rigid flows would reflect decadal changes in ρ' that are not controlled by the lower mantle but instead related to convective core dynamics.

A simple estimate of the density change associated with core flows is obtained from (22). For a typical change in flow amplitude $\mathcal{U}$, there should be an associated change in density of

$$\rho' \sim \frac{2\Omega\rho_f}{g_f}\frac{L_h}{L_z}\mathcal{U} \,, \tag{23}$$

where L_z is a typical length scale of the shear of $\mathcal{U}$ in the z-direction and L_h is a typical length scale of the horizontal gradient in ρ'. An order of magnitude estimate of the gravity variations resulting for such density heterogeneities is obtained from (11) and (12). Let us assume that density variations are concentrated in a layer of thickness δ at the top of the core. Typical changes in the Stokes coefficients are then

$$\Delta C_{lm} \sim \frac{4\pi}{(2l+1)^{3/2}}\left(\frac{r_f}{r_e}\right)^l \frac{2\Omega\rho_f r_f^2}{Mg_f}\frac{\delta}{L_z}\frac{L_h}{L_z}\mathcal{U} \,. \tag{24}$$

Using $\mathcal{U} = 0.03$ mm s^{-1}, $L_h = r_f$, $\delta/L_z = 1$ and the parameter values in Table 1, we expect a change in Stokes coefficients of 10^{-11}, 3×10^{-12} and 10^{-12} for degrees 2, 3 and 4, respectively. As for the pressure part, the density-induced gravity changes fall by approximately one order of magnitude for an increase of two in harmonic degree. This simple order of magnitude estimate suggests that, provided a thermal wind balance holds for decadal variations near the top of the core, gravity variations associated with density heterogeneities may be of the same order of magnitude as those from pressure changes at the CMB.

Furthermore, we expect gravity variations from density and pressure to be related. This relationship is brought out by taking the z-component of (18), yielding (Hulot *et al.* 1990; Jault & Le Mouël 1991)

$$\begin{aligned}\rho' &= -\frac{1}{g_f\cos\theta}\frac{\partial p}{\partial z} \,, \\ &= -\frac{1}{g_f}\frac{\partial p}{\partial r} + \frac{\tan\theta}{r\,g_f}\frac{\partial p}{\partial\theta} \,.\end{aligned} \tag{25}$$

Since (11) and (12) involve integrals in radius, the contribution from the first term on the right-hand side of (25) to the density-induced gravity variations is then directly proportional to the pressure at the CMB, with the negative sign indicating that the pressure and density contributions must partly cancel one another. The presence of the second term in (25) implies a deviation from a simple one-to-one relation between the gravity variations from pressure and density. Nevertheless, we expect the gravity signals from each contribution to be related and partly cancelling one another.

However, several objections on the reconstruction of ρ' from (22) can be raised. First, we expect the Lorentz force to be more important deeper in the core so that density can no longer be related simply to core flows. This may not completely invalidate the above approach since the integral in eqs (11) and (12) involves a factor r^{l+2} and thus gravity variations should be dominated by density heterogeneities in the outermost part of the core.

A second objection, and a more fundamental one, is that by taking the curl of the magneto-geostrophic balance, geostrophic flows are removed. These flows are rigid (invariant in z) and supported by non-axial pressure gradients,

$$2\Omega\rho_o\mathbf{u} = \hat{\mathbf{z}}\times\nabla p \,. \tag{26}$$

An illustration of a geostrophic flow is shown in Fig. 4(b). In rapidly rotating fluids, we expect rigid flows to dominate the dynamics. And based on this, observed decadal changes in core flows should include an important component of rigid motions. Relating density to flows through (22) amounts to make a *de facto* assumption that all observed changes in core flows are carried by non-rigid motions, which is contrary to our expectation of the dynamics.

If one assumes purely rigid flows, $L_z \to \infty$, and based on (23), decadal core flows should not involve any density variations: there

should be no density-induced gravity variations. As we will see in the next subsection, core flows cannot be purely rigid, and decadal variations in density are thus expected. Nevertheless, this illustrates that if decadal changes in the flow are predominantly rigid, our estimate of the density-induced gravity signal based on a simple thermal wind balance is likely to be grossly overestimated and inaccurate.

The difficulty of separating the flows at the surface of the core into its rigid and non-rigid contributions is ultimately the limiting factor in trying to recover density variations. As we discuss further in section 3, the shear of the flow near the CMB cannot be constrained robustly with geomagnetic observations, preventing a resolution of this issue from the observed secular variation. In contrast, the pressure at the CMB determined from (19) does not involve radial flow gradients; it can be determined from core surface flows regardless of the relative importance of rigid and non-rigid flows. For this reason, the pressure-induced gravity changes can be more reliably determined than the density-induced gravity changes.

Although this is outside the scope of the present work, we note that density heterogeneities determined on the basis of a thermal wind balance may be appropriate for estimating gravity variations taking place over a timescale of a thousand years. This is the timescale corresponding to one convection overturn and thus the timescale at which large scale reorganization of the density structure is expected. Over such a timescale, the magnetic field is expected to organize itself such that its shear by the flow is minimal, resulting in a quasi-steady flow pattern predominantly controlled by a thermal wind balance (e.g. Aubert 2005). Millennial timescale fluctuations in this balance would involve non-rigid flows as large as rigid flows, as indeed may be tentatively supported by observations (e.g Dumberry & Bloxham 2006).

2.2.3 Lateral density heterogeneities inferred from quasi-geostrophic flows

As mentioned in the preceding subsection, motions in the core are expected to be dominated by rigid, geostrophic flows. Such columnar flows appropriately describe convective motions near onset (e.g. Busse 1970; Dormy *et al.* 2004) and also describe reasonably well the flow regime in fully developed convection capable of maintaining a dipolar magnetic field (Olson *et al.* 1999; Christensen & Aubert 2006). This motivates us to consider a perhaps more realistic description of the dynamics, one which takes into account the predominance of geostrophic motions, in order to relate density to flow.

We thus consider core flows in the quasi-geostrophic (QG) approximation limit. Details on the QG flows and the QG approximation for the dynamics can be found for instance in Cardin & Olson (1994), Aubert *et al.* (2003) and Gillet & Jones (2006). QG motions are more aptly described in a cylindrical reference frame (s, ϕ, z). The leading order flow $\mathbf{u}^0 = \mathbf{u}^0(s, \phi)$ is invariant in z and satisfies a geostrophic balance,

$$2\Omega\rho_o \mathbf{u}^0 = \hat{\mathbf{z}} \times \nabla p \,. \tag{27}$$

The leading order quasi-geostrophic flow is thus identical to the geostrophic flow illustrated in Fig. 4(b).

Since in a spherical geometry such flows cannot satisfy the condition of impermeability at the boundaries, a secondary flow $\mathbf{u}^1$ is required. This flow involves an axial component u_z^1 which is purely non-rigid ($\partial u_z^1/\partial z \neq 0$). The force balance at the next order gives the dynamic evolution of $\mathbf{u}^0$ in relation to the secondary flow $\mathbf{u}^1$. It is written as an equation for the evolution of the axial vorticity $\zeta = \hat{\mathbf{z}} \cdot \nabla \times \mathbf{u}^0$,

$$\frac{\mathrm{D}\zeta}{\mathrm{D}t} - 2\Omega\rho_o \frac{u_z^1(H)}{H} = \frac{g_f}{r_f}\frac{\partial [\rho']_z}{\partial \phi} + [\hat{\mathbf{z}} \cdot \nabla \times (\mathbf{J} \times \mathbf{B})]_z \,, \tag{28}$$

where

$$\frac{\mathrm{D}}{\mathrm{D}t} \equiv \frac{\partial}{\partial t} + \mathbf{u}^0 \cdot \nabla_e \,, \qquad \nabla_e \equiv \frac{\partial}{\partial s} + \frac{1}{s}\frac{\partial}{\partial \phi} \,, \tag{29}$$

and where we have used the notation

$$[X]_z = \frac{1}{2H}\int_{-H}^{H} X \,\mathrm{d}z \,, \tag{30}$$

with $H = \sqrt{r_c^2 - s^2}$. The no-penetration condition at the CMB allows to relate the axial flow $u_z^1(H)$ to the s-component of the leading order flow by $u_z^1(H) = -s u_s^0/H$. Thus,

$$\frac{\mathrm{D}\zeta}{\mathrm{D}t} + 2\Omega\rho_o \frac{s\, u_s^0}{H^2} = \frac{g_f}{r_f}\frac{\partial [\rho']_z}{\partial \phi} + [\hat{\mathbf{z}} \cdot \nabla \times (\mathbf{J} \times \mathbf{B})]_z \,. \tag{31}$$

Eq. (31) allows us to retrieve the axially averaged density structure in the core, provided we know $\mathbf{u}^0$ and $\mathbf{B}$. If we neglect the inertial and Lorentz terms, we retrieve a simple relationship between core flows and density heterogeneities,

$$\frac{2\Omega\rho_o}{g_f}\frac{s\, u_s}{H^2} = \frac{1}{r_f}\frac{\partial [\rho']_z}{\partial \phi} \,. \tag{32}$$

Taking again $\mathcal{U}$ as a typical change in flow amplitude and L_h a typical horizontal length scale of density heterogeneities, the balance (32) should lead to a change in the axially averaged density of

$$[\rho']_z \sim \frac{2\Omega\rho}{g_o}\frac{L_h s}{H^2}\mathcal{U} \,. \tag{33}$$

Taking $s \sim H \sim r_f$, the density change from this estimate differs from that of the "thermal wind" scenario (eq. 23) by a factor L_z/r_f. If we assume $L_z \sim r_f$, we retrieve a similar estimate of density variations.

Because of the alignment in the density structure in z in the QG scenario, the integration in the radial direction in eqs (11) and (12) involves a mixture of the different harmonic components of the density determined at the CMB. However, because of the factor r^{l+2} in the gravity integrals, density heterogeneities in the outermost part of the core should dominate gravity variations. For the lowest harmonic degrees, whether the projection of the CMB density is radial or axial should not alter the amplitude of the gravity prediction significantly. We will see in the next section that this is indeed the case.

The problem with neglecting inertia and the Lorentz force in (31) is that it amounts to assuming that changes in the QG flows are entirely driven by changes in the secondary, non-rigid axial flow in response to fluctuations in the axially averaged density. In other words, assuming (32) is equivalent to assuming once more that the non-rigid flow dynamics dominates observation. This is contrary to the underlying assumption of QG motions. Indeed, even in the absence of the Lorentz force, convective QG flows involve a balance between inertia, the Coriolis term and buoyancy in (31) (e.g. Gillet & Jones 2006). Hence, it is difficult to justify removing the inertial term. For the balance appropriate for the Earth's core, there is also no justification to remove the Lorentz force. Furthermore, the addition of the Lorentz force allows Alfvén waves and Magnetic–Coriolis (MC) waves to propagate. These waves do not involve density and may comprise an important part of the decadal core flow variations.

With inertia and the Lorentz force actively contributing to the force balance, the unfortunate implication is that it becomes much more difficult to relate ρ' simply in terms of core flows. A dynamic relationship between ρ' and core flows accounting for the Lorentz force may be derived, but non-uniqueness is likely to be a serious issue and this is outside the scope of this work. For lack of a better way, we use (32) in the next section to obtain estimates of density variations. However, it will have to be kept in mind that using this balance gives an upper bound for possible density heterogeneities in the core that are compatible with core flows. We expect that, in a QG scenario, they should be much smaller.

3 PREDICTED VARIATIONS IN GRAVITY FROM THE SECULAR VARIATION OF THE MAGNETIC FIELD

We now present an attempt at reconstructing gravity variations from core flows that have taken place between 1900 and 1990. We follow the traditional approach in geomagnetism: we recover core flows from the secular variation of the geomagnetic field based on the approximation of frozen flux (Roberts & Scott 1965; Backus 1968). At the CMB, where we impose the condition $u_r = 0$, the poloidal component of the induction equation under the frozen flux approximation is

$$\frac{\partial \mathbf{B_P}}{\partial t} = \boldsymbol{\nabla} \times (\mathbf{u} \times \mathbf{B_p}), \tag{34}$$

where $\mathbf{B}_\mathrm{p}$ is the poloidal part of the magnetic field at the CMB. The latter is known from a downward continuation of the field at the surface of the Earth to the CMB. The radial component of this equation is

$$\frac{\partial B_r}{\partial t} = -\boldsymbol{\nabla}_h \cdot (B_r \mathbf{u}_h), \tag{35}$$

where B_r is the radial component of the magnetic field.

Gravity variations require the knowledge of the variations in pressure at the CMB and the variations in density inside the core. To recover the pressure at the CMB from (19), only the knowledge of $\mathbf{u}_\mathrm{h}$ is required and can be obtained by inverting (35). To recover density, one strategy is to assume that the observed decadal changes in $\mathbf{u}_\mathrm{h}$ reflect changes in non-rigid flows driven by density variations (the 'thermal wind' scenario). In this case, density variations can be obtained from (22), which requires the knowledge of axial gradients in the flow. These can be obtained by inverting both the radial and horizontal components of the poloidal induction equation in (34) simultaneously. This was the strategy adopted by Jackson & Bloxham (1991) in order to recover the steady thermal wind component of the flow.

A second strategy to recover density variations is to assume instead that decadal variations in core flows are described by QG motions. In this case, the geometry of the flow inside the core is entirely determined by the flow at the surface of the core. Both the pressure variations at the CMB (from eq. 19) and the axially averaged density variations (from eq. 32, if one neglects inertia and the Lorentz force) can be retrieved from $\mathbf{u}_\mathrm{h}$, which is obtained from an inversion of (35) alone.

3.1 The thermal wind scenario

Let us first consider the thermal wind scenario. Solutions to (34) suffer from non-uniqueness. A part of this non-uniqueness is alleviated by constraining the flows and the shear to satisfy conditions deriving from the assumption of tangential geostrophy near the surface of the core. Taking $\boldsymbol{\nabla}_h \cdot$ (19) leads to

$$\boldsymbol{\nabla}_h \cdot (\mathbf{u_h} \cos\theta) = 0 \tag{36}$$

whereas taking $\boldsymbol{\nabla}_h \cdot$ (22) leads to,

$$\boldsymbol{\nabla}_h \cdot (\mathbf{u}' \cos\theta) = \boldsymbol{\nabla}_h \cdot (\sin\theta \boldsymbol{\nabla}_h \cdot \mathbf{u_h}\hat{\theta}), \tag{37}$$

where $\mathbf{u}' = \frac{\partial \mathbf{u}}{\partial r}$. A discussion on the uniqueness of the flow and shear solutions derived from these constraints is presented in Jackson & Bloxham (1991). However, with this scheme, the shear of the flow is not really constrained by the secular variation through (34); rather, it is simply related to the flow through (37). This is because the poloidal magnetic field can be defined in terms of a potential V through $\mathbf{B} = -\boldsymbol{\nabla} V$. Since the evolution of V can be determined from the radial part of the induction equation alone (eq. 35), no additional information can be expected from the tangential part of (34) (Jault & Le Mouël 1991; Whaler & Davis 1997, A. Jackson, personal communication, 2009). Thus, applying the above constraints does not constitute a true recovery of the shear, but instead determines the shear such that it is consistent with the purely non-rigid flows of the thermal wind scenario.

We could have chosen to reduce the non-uniqueness by using different constraints than (36) and (37), for example that the flow must be toroidal (e.g. Whaler 1980) or helical (Amit & Olson 2004). Details on the different flow constraints can be found in many studies, notably in the review articles by Bloxham & Jackson (1991) and Holme (2007). The advantage of the above choice is one of self-consistency; the assumptions used to derive the flows and and shear are the same as those which allow to relate them to p and ρ'.

We construct solutions at fixed epochs between 1900 and 1990 by following the method described in Jackson & Bloxham (1991). Our solutions are based on the geomagnetic field model *gufm1* of Jackson *et al.* (2000). Besides conditions (36) and (37), we constrain the flow and the shear to satisfy regularization conditions on spatial gradients at the CMB, applying the same damping parameter for both. We chose the damping parameter such that the time-averaged flow and shear during the interval 1960–1980 are similar to the solution presented in (Jackson & Bloxham 1991, their fig. 4).

Based on this flow model, we retrieve the temporal changes in pressure at the CMB from (19). Associated variations in gravity are determined from (14) and (15). Similarly, temporal changes in density near the surface of the core are obtained from (22). The associated variations in gravity can be determined from (11) and (12), though here we need the density changes deeper in the core, not only near the CMB. Because we do not know how the shear in the flow varies deeper in the core, we make the simplest possible choice: we assume that density is radially invariant in a layer of thickness δ and identically zero below that depth. This is equivalent to assuming that the integrated gravity signal from density anomalies below a distance δ from the CMB cancels itself out.

We select a value of δ equal to 1000 km. This choice is motivated by the fact that the amplitude of the gravity signal increases approximately linearly with δ up to a depth of approximately 1000 km, at which point a further increase in δ no longer leads to substantial increase in gravity. Choosing $\delta = 1000$ km then allows to get an approximate upper bound for the gravity signal, while making it easy to scale the predicted gravity signal for smaller values of δ.

Fig. 5 shows the predicted variations in Stokes coefficients of degrees 2, 3 and 4 between 1900 and 1990 based on our inverted flow and shear model. On all plots, a time-averaged value has been subtracted. Because of the non-uniqueness of core flows and assumptions built into the inversion method, the predictions on Fig. 5

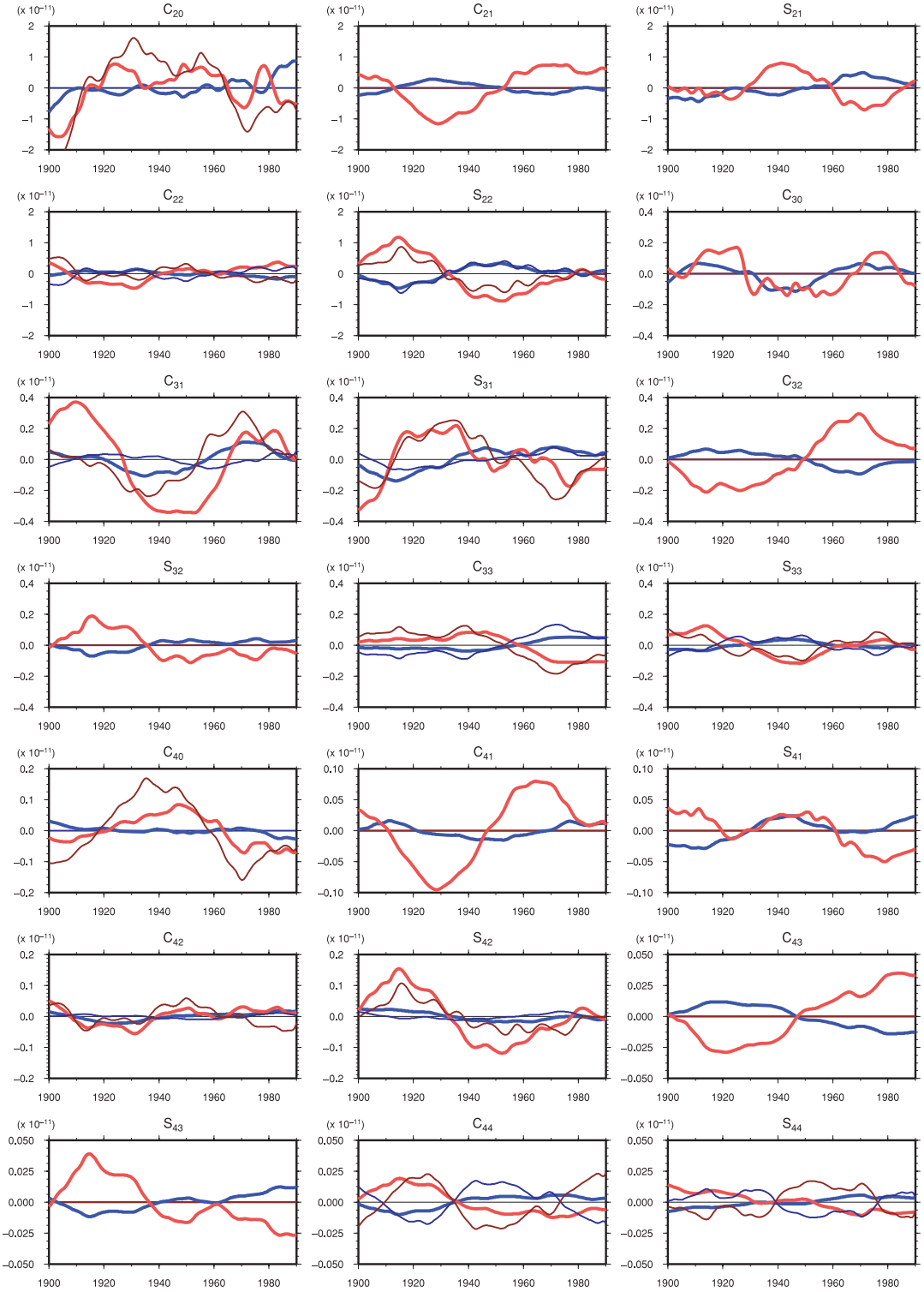

Figure 5. Predicted changes in Stokes coefficients C_{lm} and S_{lm} for degree 2, 3 and 4 between 1900 and 1990. The predictions shown are those from pressure variations at the CMB computed from (14) and (15) for the thermal wind scenario (thick red lines) and for QG flows (thin darker red lines), and those from density heterogeneities in the core computed from (11) and (12) for the thermal wind scenario (thick blue lines) and for QG flows (thin darker blue lines). A time-averaged component has been subtracted from all plots. The horizontal axis for all plots is calendar year.

should be viewed as representing an approximate indication of the expected variations rather than an accurate prediction.

A part of the geomagnetic secular variation occurs with a typical timescale of a few decades and therefore, our reconstructed core flows have typical variations on the same timescale. These lead to the predicted decadal variations in gravity in Fig. 5. The pressure-induced variations in the Stokes coefficients on Fig. 5 (thick red lines) are of the order of 10^{-11}, 3×10^{-12} and 10^{-12} for harmonic

degrees 2, 3 and 4, respectively. This is in broad agreement with our estimates in Section 2.2.1 These represent equivalent geoid height variations of approximately 0.15, 0.05 and 0.02 mm, and changes in gravity of 70, 30 and 15 nGal, respectively. The decrease in amplitude with increasing harmonic degree is dominantly caused by the progressively smaller values of $\bar{k}_l$; the pressure variations at the CMB are of the same order, approximately 100 Pa, for degrees 2, 3 and 4.

Typical gravity variations caused by density heterogeneities (thick blue lines on Fig. 5) are of the same order as those from pressure, though smaller by approximately a factor 2. This is again in broad agreement with our estimate in Section 2.2.2 These gravity variations are function of our choice of δ: for $\delta < 1000$ km, their amplitude decrease approximately linearly with δ.

We also note that the gravity signal from pressure and density tend to be anticorrelated, though this is not always the case. This is expected from the relationship between pressure and density in (25). The anticorrelation is also expected on physical grounds. Regions of low (high) density in the core should correspond to upwellings (downwellings) and to regions of high (low) pressure at the CMB. Thus, areas of negative (positive) gravity anomalies from low (high) density should coincide with areas of positive (negative) gravity anomalies caused by the uplift (depression) of the CMB and associated elastic deformations. This is analogous to the gravity anomalies associated with mantle convection, where topographic highs (lows) at density discontinuities are dynamically maintained by the upwelling (downwelling) associated with low (high) density, leading to anticorrelated gravity signals from the volumetric density part and topography part (Hager *et al.* 1985, 1989; Defraigne *et al.* 1996). In the case of mantle convection, the topography defections are maintained by viscous stresses; CMB deflections from core flows are instead maintained by pressure gradients. Because of this anticorrelation, in a thermal wind scenario, the overall gravity signal induced by core flows is smaller than its individual contributions from pressure and density.

We note that although the anticorrelation is consistent with our physical intuition, this should not be taken as an indication that the shear component of the flow that we have retrieved is correct. Rather, it merely illustrates that the shear is consistent with the imposed constraints.

3.2 The quasi-geostrophic scenario

Let us now consider gravity variations when motions in the core are approximated by QG flows. In this case, non-uniqueness in the flows inverted from (35) is reduced by requiring the flow to satisfy the condition of tangential geostrophy but also to constrain flows outside the tangent cylinder to be symmetric with respect to the equator. Flows inside the tangent cylinder, above and below the inner core, are separated by the latter and are not imposed to be equatorially symmetric. Details of these constraints and of their implementation in an inversion scheme can be found in Pais & Jault (2008).

We use here a QG flow model, based on *gufm1*, representing an average of many inversions that take into account in a stochastic manner the interaction between core flows and hidden small scale magnetic field at the CMB. More details on similar flow models can be found in Gillet *et al.* (2009).

The QG pressure is determined from tangential geostrophy (eq. 19). If we neglect inertia and the Lorentz force, the internal density structure is directly related to internal core flows by (32). (A slightly altered form is used inside the tangent cylinder to take into account the presence of the inner core.) Since in the QG approximation the flow geometry everywhere inside the core is specified by surface core flows, the integral over density in the core (11 and 12) can be evaluated from the ICB to the CMB. It has to be kept in mind though that the retrieved QG density is the axially averaged component, so an assumption about the axial distribution of density is nonetheless required. We make the simplest possible choice and assume that the density is axially uniform.

The gravity variations predicted on the basis of the QG flow solution is shown on Fig. 5: the pressure-induced variations are depicted by the thin dark red lines, and the density-induced variations by the thin dark blue lines. The gravity predictions are different than those obtained in the thermal wind scenario. This is because of the different constraints imposed on core flows. The most notable difference concerns coefficients of harmonics that are equatorially anti-symmetric, such as $(l = 2, m = 1)$, $(l = 3, m = 0)$, $(l = 3, m = 2)$, etc. The geometry of the QG flows forces the CMB pressure and the density structure outside the tangent cylinder to be symmetric about the equator. As a consequence, predicted gravity variations are very small for equatorially antisymmetric coefficients (they are not exactly zero because the equatorial symmetry is broken by flows inside the tangent cylinder).

Other than this main difference, while some Stokes coefficients predictions remain very different from those derived using the thermal wind scenario (e.g. S_{44}), some are very similar (e.g. S_{22}) both in amplitude (confirming the order of magnitude analysis of Section 2.2.3) and in the details of the variations. This is perhaps surprising, especially for the density-induced part, given that they are derived from different diagnostic equations (eq. 22 versus eq. 32). This illustrates how the condition (32) is similar to condition (22). Since the latter is derived with the built-in assumption that decadal variations are dominated by non-rigid flows, the implication is that (32) is appropriate when the dynamics in the QG case are also controlled by the non-rigid part of the flow. In other words, that in both cases, decadal flow changes are purely driven by changes in density.

As in the thermal wind scenario, the pressure and density contributions to the gravity signal are generally anticorrelated. The physical reasoning is the same. Hence, if decadal density changes are important, and dominantly responsible for changes in core flows, the pressure-induced and density-induced gravity contributions partly cancel one another. If, however, geostrophic flows dominate the dynamics at decadal timescales (e.g. Jault 2008), our confidence in the density retrieved from (32) is very low. We expect the gravity variations from density to have a smaller amplitude than those shown in Fig. 5. Thus, the gravity signal should be dominated by the contribution from pressure changes at the CMB.

The gravity predictions that are presented in Fig. 5, for both scenarios, are based on a purely elastic mantle. However, the lowermost mantle (D'') may deform viscously on a decadal timescale on account of its higher temperature than the rest of the mantle (e.g. Lay *et al.* 2008). Allowing for viscous deformations, one expects larger deformations of the CMB, and thus a larger gravity signal, for a given pressure change at the CMB. To obtain an estimate of this increase, we have modelled the entire D'' region as a fluid and moved the solid–fluid boundary to the top of D''. For such an earth model, the computed values of $\bar{k}_l$ are larger, though only modestly; we found an increase in $\bar{k}_2$ of 23 per cent. The changes are not larger because, although a larger displacement of the CMB is allowed when D'' is fluid, deformations remain elastic in the lower mantle and this limits the amplitude of the CMB displacement. Since viscous deformations in D'' over decadal timescales are likely much smaller than for

our fluid D'' scenario, they should not lead to significant increase in gravity. This also suggests that gravity variations produced by core flows cannot be used to monitor the anelastic properties of D''.

3.3 Zonal gravity variations

A few words are in order for the zonal components of the gravity changes expressed by the coefficients C_{l0}. These are related to time-dependent zonal flows at the surface of the core. This is the part of the flow for which we have the greatest confidence; changes in the core angular momentum calculated on their basis correspond well with those required to explain the observed variations in the length of day (LOD) (Jault *et al.* 1988; Jackson *et al.* 1993). One assumption that enters this calculation is that these time-dependent flows are geostrophic, that is, purely rigid inside the core. If this is so, they are supported by axially symmetric radial pressure variations alone. Thus, there should be no contribution to the gravity variation from axially symmetric density. In fact, this emerges naturally under the QG approximation: the right-hand side of (32) is zero for the axially symmetric density and thus it cannot contribute to flow.

The zonal part of the tangentially geostrophic flows that we have used in the thermal wind scenario in Fig. 5 is not symmetric about the equator. This can be seen for instance in the pressure contribution to C_{30}, which would be zero for purely rigid flows (it is almost zero for the QG flow). This is perhaps evidence of non-rigid variations on decadal timescale in the core, though this could also simply reflect imperfections of the flow model. Since the presence of non-rigid flows can improve the fit with the LOD variations and would indicate that decadal motions in the core depart from quasi-geostrophy, determining the relative contributions from rigid and non-rigid parts of the zonal flow is an important issue.

This could be settled by gravity observations. Dominantly rigid flows would result in odd-degree zonal Stokes coefficients much smaller than the even degree ones. In addition, since rigid flows are only supported by pressure changes, the prediction of gravity variations that they produce can be much more reliably determined. A comparison between observed and predicted zonal gravity variations of even degree should then further help to confirm the nature of the zonal flows in the Earth's core.

3.4 C_{21}, S_{21} coefficients and polar motion

The coefficients C_{21} and S_{21} are directly related to the change in the moment of inertia tensor of the Earth. These changes lead to variations of the orientation of the Earth's rotation vector with respect to the mantle or, more simply, to polar motion. Indeed, the idea that pressure variations at the CMB may entrain polar motion through a combination of a change in the moment of inertia and an equatorial torque on the mantle (by topographic coupling at the CMB) has been investigated by many authors (e.g. Hinderer *et al.* 1987, 1990; Greff-Lefftz & Legros 1995; Hulot *et al.* 1996; Hide *et al.* 1996). The general conclusion of these studies is that the predicted polar motion is too small by approximately a factor 5–10, in the best of cases, to explain the observed decadal variations in polar motion.

We do not wish to present here an updated calculation of the polar motion. The amplitude of our predicted variations in C_{21} and S_{21} in the thermal wind scenario, together with the torque at the CMB, would lead to a decadal polar motion of the same order of magnitude as found in the above studies. In fact, it should be even smaller, for these above studies did not consider the density contribution to the changes in the moment of inertia and only the study of Hulot *et al.* (1996) discussed the density part of the torque between the core and mantle. Since for both the moment of inertia and the torque the density contribution should partly cancel the pressure contribution, the resulting polar motion should be smaller.

It is worth pointing out that if core flows are close to being quasi-geostrophic, the equatorial symmetry of such flows implies that the resulting C_{21} and S_{21} variations should be much smaller, as can be seen in Fig. 5. The equatorial topographic torque on the mantle, of which the dominant part is from the interaction between $l = 2, m = 1$ pressure interacting with the equatorial bulge, would also be much smaller than in the thermal wind scenario. Interactions between equatorially symmetric flows and equatorially antisymmetric parts of the CMB topography, h^A, can still generate a topographic torque (e.g. Hinderer *et al.* 1990), though smaller by a factor of h^A over the amplitude of the equatorial bulge at the CMB. Thus, if core flows are approximately quasi-geostrophic, the polar motion that they can produce would be too small by at least two orders of magnitude to explain the observed decadal variations.

4 PREDICTED VERSUS OBSERVED GRAVITY CHANGES

Surface processes are responsible for interannual gravity changes of approximately 5×10^{-11} in the Stokes coefficients of low harmonic degrees (e.g. Chen & Wilson 2005, and also Fig. 6). However, according to the work of Chen *et al.* (2005), surface processes cannot explain the variations in the degree 2 coefficients at a timescale of 10 yr and more. This may be due to modelling deficiencies, but it may also indicate that the signal is from a different origin. In order to verify whether a gravity contribution from core flows can be detected in gravity observations, and perhaps even explain a part of the observed signal, we need to compare our prediction with a model of observed gravity variations.

A model of the temporal variations in C_{lm} and S_{lm} for harmonic degree 2 and 3 as determined by Satellite Laser Ranging (SLR) is shown in Fig. 6 (grey lines). This model is an updated version of the one presented in Cox *et al.* (2004), and after a correction for the IB-NCEP atmospheric gravity series (C. M. Cox, personal communication, 2006). The Stokes coefficients in this model represent monthly averages, with errors of the order of 10^{-11}.

Annual variations of approximately 10^{-10} in amplitude are clearly visible for all Stokes coefficients. This signal is driven by a combination of atmospheric, oceanic, and hydrological seasonal mass variations (Cox & Chao 2002; Chen & Wilson 2003). Interannual variations of up to a few years, with an amplitude of the order of 2×10^{-11} are also caused predominantly by mass variations at the Earth's surface (Chao *et al.* 2003; Chen *et al.* 2005). Also observed are longer temporal trends, most clearly in the coefficients C_{20} and S_{21}. The secular trend in C_{20} is a result of the change in the ellipticity of the Earth caused by postglacial rebound (Yoder *et al.* 1983; Rubincam 1984; Mitrovica & Peltier 1993). The secular trend in S_{21} (and in C_{21} though it is less visible) correspond to the change in the Earth's moment of inertia from postglacial rebound (Peltier & Jiang 1996) and also mantle convection (Steinberger & O'Connell 1997).

Variations at a timescale of 5–10 yr and of the order of 5×10^{-11} are also clearly visible in Fig. 6. These 'decadal' variations are shown by the black curves, obtained by applying a third order low-pass Butterworth filter with a period threshold of 5 yr to the SLR model.

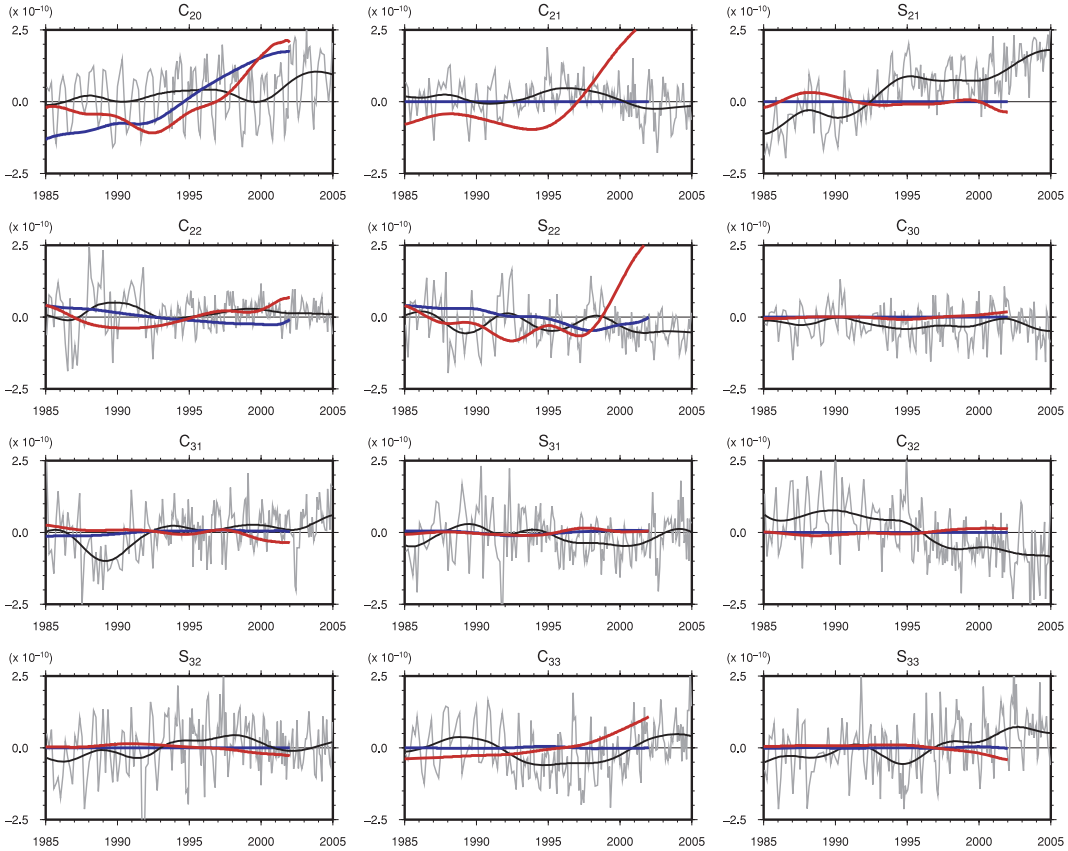

Figure 6. Temporal variations in Stokes coefficients C_{lm} and S_{lm} of degree 2 and 3 between 1985 and 2005 based on a model reconstructed from SLR tracking by Cox *et al.* (2004) (grey lines). Decadal variations (black lines) are obtained by applying a third order low-pass Butterworth filter with a period threshold of 5 yr to the SLR model. Also shown are predictions of the variations from pressure changes at the CMB, based on tangentially geostrophic flow model (red lines) and a QG flow model (blue lines). To improve visibility, these two predictions have been multiplied by a factor 10. A time-averaged component has been subtracted from all plots. The horizontal axis for all plots is calendar year.

Predictions from core flows are also shown on Fig. 6. Since the gravity signal from density heterogeneities is less reliably retrieved than that from pressure changes at the CMB, and likely smaller, to simplify, we computed only the pressure-induced gravity prediction. The red lines on Fig. 6 are predictions from a core flow model constrained to satisfy tangential geostrophy. The blue lines are predictions based on a QG flow model. The latter is an average flow from many inversions that incorporate a small-scale magnetic field in a stochastic manner (Gillet *et al.* 2009). Both flow models are inverted using (35) and based on the geomagnetic model CM4 (Sabaka *et al.* 2004), which covers the period 1960–2002.

To render more visible the details of these two predictions on the scale of Fig. 6, they have been multiplied by a factor 10. The predicted variations are smaller than the observed variations by an order of magnitude for degree 2, and smaller by an even larger factor for degree 3. Moreover, there is no indication of a correlation between the predicted and observed signals.

If interannual gravity variations were caused by core flows, we expect a decrease in their amplitude for increasing harmonic degree. This is not the case: the amplitude of the observed interannual variations on Fig. 6 are similar for degree 2 and 3 (and also degree 4, not shown). This is evidence that the interannual gravity variations of the order of 5×10^{-11} are most likely caused by surface processes rather than by pressure changes at the CMB.

This implies that it is at present not possible to use gravity data to determine the relative contributions of rigid and non-rigid parts of the zonal flows at the surface of the core, as we suggested in Section 3.3. Similar conclusions had been reached by Dumberry & Bloxham (2004) and Greff-Lefftz *et al.* (2004).

Though the observed interannual gravity changes in Fig. 6 are unlikely to be caused by core flows, they can be used to place upper bounds on the interannual pressure variations of low degree at the CMB, as was first attempted two decades ago by Merriam (1988). The largest observed variations in the Stokes coefficients of degree 2 over the last 20 yr, discounting the secular change in the moment of inertia responsible for the changes in C_{21} and S_{21}, are approximately 5×10^{-11}. This corresponds to a pressure change at the CMB of approximately 350 Pa. In order to produce such a pressure change, variations in the flow at the surface of the core of approximately 0.07 mm s^{-1}, or 2.2 km yr^{-1} are required. Taking 5 yr as a typical time for the observed interannual gravity changes, this corresponds to accelerations of 0.44 km yr^{-2}. This is well within the bounds of the flow determined from the secular variation. Larger accelerations over a 5 yr time span would lead to larger than observed gravity variations. It is important to stress that this upper bound estimate on the change in flow is purely based on the observed gravity variations and is completely independent of that obtained from the observed geomagnetic secular variation.

Since the pressure-induced gravity signal vary approximately as $3^{-l}(2l+1)^{-1/2}$ with increasing harmonic degree l, similar upper bounds for higher degrees are less useful as the allowed change in flow speed becomes rapidly orders of magnitude larger than that derived from the secular variation. For instance, at degree 3, the upper bound on interannual pressure changes are approximately 1400 Pa corresponding to a maximum change in the flow of 0.28 mm s^{-1}, or 8.5 km yr^{-1}. This means that gravity variations cannot be used to constrain the amplitude of small scale flows at the CMB which may participate in the observed large scale secular variation of the magnetic field (e.g Eymin & Hulot 2005).

A similar exercise allows us to estimate the largest density variations within the core that have taken place in the past two decades. We calculate this estimate by using radially invariant density heterogeneities in the integrals of (11) and (12). At degree 2, the observed change of 5×10^{-11} in the Stokes coefficients imposes an upper bound of $\rho' \sim 10^{-3}$ kg m^{-3}, or $\rho'/\rho_o \sim 10^{-7}$. If there are large cancellations in the gravity integral, or if the heterogeneities are concentrated in the deeper part of the core, larger density anomalies are allowed. Since the density-induced gravity signal varies approximately as $2^{-l}(2l+1)^{-3/2}$ with increasing harmonic degree l, the higher the spherical harmonic degree, the larger the density heterogeneity can be: at degree 3, we find $\rho' \sim 4 \times 10^{-3}$ kg m^{-3}. We note that these estimates do not depend on any dynamic assumptions.

5 DISCUSSION AND CONCLUSION

In this work, we have computed predictions of gravity changes during the past century caused by pressure variations at the CMB and by temporal variations in density heterogeneities within the fluid core. Both of these predictions are based on temporal variations of flows at the surface of the core reconstructed from the geomagnetic secular variation.

Our results suggest that typical gravity variations from pressure changes over decade timescales are expected to be of the order of 70, 30 and 15 nGal for harmonic degrees 2, 3 and 4, respectively. These correspond to equivalent changes in geoid height of 0.15, 0.05 and 0.02 mm, respectively. The amplitude of the gravity variations from decadal variations in density within the core is more difficult to evaluate solely based on flows at the surface of the core. If these flows are predominantly driven by decadal density variations, the amplitude of the density-induced gravity variations should be similar than that from pressure. We also expect the two contributions to be anticorrelated because regions of low (high) density in the core should correspond to upwellings (downwellings) and be associated with a high (low) pressure at the CMB. Thus, regions of negative (positive) density-induced gravity anomaly should coincide with regions of positive (negative) pressure-induced gravity anomaly caused by the uplift (lowering) of the CMB. The overall gravity variations resulting from core flows would then be much reduced than the above quoted values. However, if decadal core flows reflect primarily the dynamics of axially invariant geostrophic motions, the density-induced gravity variations should be significantly smaller than the pressure-induced part.

To gain a better understanding of the role of density in time-dependent core flows, one option is to use numerical models of the geodynamo. This is the strategy followed in the study of Jiang *et al.* (2007), where gravity variations from CMB pressure and density variations in the core are computed based on one such model. They find that the pressure contribution dominates for axisymmetric harmonics, but that the contributions from density and pressure are approximately equally important for the non-axisymmetric harmonics. Though their results apply for gravity anomalies at the CMB, and not at the Earth's surface, the implication is that non-zonal core flows in the model appear to be primarily driven by density changes. Applying these conclusions to Earth, we should then expect the gravity signal from pressure and density to largely cancel one-another. However, care has to be taken when relating the results of such simulations to Earth. The large contribution from density to the total gravity signal in the model may reflect an inappropriate scaling of density heterogeneities. Additionally, the timescale of the variations in the model, when scaled to the Earth, correspond to a few thousand years. The gravity variations investigated by Jiang *et al.* (2007) thus pertain to a much longer timescale than that of decades, our timescale of interest in the present study. Variations in non-rigid flows are expected to occur in the Earth over a timescale of a few thousand years (e.g. Aubert 2005; Dumberry & Bloxham 2006). If their amplitude is as large as that of rigid flows, we indeed expect that the gravity contribution from density may be similar to that from pressure, as suggested by our order of magnitude estimate in Section 2.2.2 Further numerical efforts are required to determine the relative importance of pressure and density-induced gravity variations.

The observed interannual variations in the Stokes coefficients of low degrees for the interval 1985–2005 are of the order of 5×10^{-11} as shown on Fig. 6. These are most likely produced by surface processes rather than induced by core flows. Nevertheless, these observed variations allow to place upper bounds in pressure change at the CMB and density change within the core that have taken place during the past 20 yr. For degree 2, we find a maximum pressure change of approximately 350 Pa and a maximum departure from hydrostatic density of approximately 1 part in 10^7, though this latter value could be larger if there are significant radial variations in the non-hydrostatic density. Both of these estimates are derived solely from gravity observations; they do not dependent on dynamic assumptions or on the observed magnetic field secular variation.

The estimate for density variations is important in the context of the recent study by Dai & Song (2008), where the presence of heterogeneous, time-dependent outer core structures is postulated in order to explain the observed temporal variations in the waveform of earthquake doublets. For large-scale structures ($\sim$1000 km), variations of seismic wave speed of the order of 0.01 per cent are required to explain observations. If these are caused by a change in density, this would correspond to variations of $\rho'/\rho_o \sim 10^{-4}$ (much larger than our above upper bound of 10^{-7}) and associated changes in Stokes coefficients of the order of 5×10^{-8}, three orders of magnitude larger than the observed gravity changes. Thus, if the seismically inferred time-dependent outer core structures are real, they cannot be explained simply in terms of density variations as the gravity variations that these would produce are too large to be compatible with observations.

The amplitude of the predicted variations in Stokes coefficients from core flows (Fig. 5) is much smaller than the typical variations caused by surface processes, which are of the order of 10^{-10} (see Fig. 6). In fact, the predicted changes that we have computed at degree 4 are below the level of precision obtained with the satellite mission GRACE, which is of the order of a fraction of 1 mm in geoid height (e.g. Tapley *et al.* 2004). Therefore, there is little hope that variations of degree 4 and larger caused by pressure changes at the CMB can be detected by GRACE.

However, at least in theory, GRACE may be capable to retrieve the gravity signature at degree 2 and 3 from pressure changes at the

CMB. Of course, since the gravity signal from the core is expected to vary over a decadal timescale, GRACE-like quality observations over a similar time span are required to do so. The greater challenge though would be to explain and remove the larger gravity variations that are caused by surface processes. Only once this is achieved, and to a level of precision of an equivalent geoid height of 0.1 mm, can we hope to observe the signal from the core.

Future improvements in gravity observations and in the modelling of surface processes may allow the contribution to gravity variations from core flows to be detectable. If so, predictions such as those presented in this work may provide further knowledge on core surface flows of low harmonic degree. Thus, gravity variations may eventually provide a way to confirm or constrain core flows recovered from the geomagnetic secular variation, thereby alleviating a part of the non-uniqueness in core flow models.

ACKNOWLEDGMENTS

I wish to express my gratitude to Christopher M. Cox for sharing his SLR gravity field model, to Andrew Jackson for sharing his inversion routines, to Nicolas Gillet for sharing his QG flow models, and to Richard Holme for providing re-formatted versions of the CM4 field models. A part of this work was completed while being supported by a NERC postdoctoral fellowship of the UK. I am currently supported by a NSERC/CRSNG discovery grant.

REFERENCES

Agnew, D.C., 2007. Earth tides, in *Treatise on Geophysics*,Vol. 3, Chap. 4, pp. 163–195, eds Schubert, G. & Herring, T., Elsevier, Amsterdam.

Amit, H. & Olson, P., 2004. Helical core flows from geomagnetic secular variations, *Phys. Earth planet. Inter.,* **147,** 1–25.

Amit, H. & Olson, P., 2006. Time-averaged and time-dependent parts of core flow, *Phys. Earth planet. Inter.,* **155,** 120–139.

Aubert, J., 2005. Steady zonal flows in spherical shell fluid dynamos, *J. Fluid Mech.,* **542,** 53–67.

Aubert, J., Gillet, N. & Cardin, P., 2003. Quasigeostrophic models of convection in rotating spherical shells, *Geochem. Geophys. Geosyst.,* **4,** 1052, doi:10.1029/2002GC000456.

Backus, G.E., 1968. Kinematics of geomagnetic secular variation in a perfectly conducting core, *Phil. Trans. R. Soc. Lond., A,* **263,** 239–266.

Bloxham, J. & Jackson, A., 1990. Lateral temperature variations at the core-mantle boundary deduced from the magnetic field, *Geophys. Res. Lett.,* **17,** 1997–2000.

Bloxham, J. & Jackson, A., 1991. Fluid flow near the surface of Earth's outer core, *Rev. Geophys.,* **29,** 97–120.

Busse, F.H., 1970. Thermal instabilities in rapidly rotating systems, *J. Fluid Mech.,* **44,** 441–460.

Cardin, P. & Olson, P., 1994. Chaotic thermal convection in a rapidly rotating spherical shell: consequences for flow in the outer core, *Phys. Earth planet. Inter.,* **82,** 235–259.

Chao, B.F., Au, A.Y., Boy, J.-P. & Cox, C.M., 2003. Time-variable gravity signal of an anomalous redistribution of water mass in the extratropic Pacific during 1998–2002, *Geochem. Geophys. Geosyst.,* **4,** 1096, doi:10.1029/2003GC000589.

Chen, J.L. & Wilson, C.R., 2003. Low degree gravitational changes from earth rotation and geophysical models, *Geophys. Res. Lett.,* **30,** 2257, doi:10.1029/2003GL018688.

Chen, J.L. & Wilson, C.R., 2005. Hydrological excitation of polar motion, 1993–2002, *Geophys. J. Int.,* **160,** 833–839.

Chen, J.L., Wilson, C.R. & Tapley, B.D., 2005. Interannual variability of low-degree gravitational change, 1980–2002, *J. Geod.,* **78,** 535–543.

Christensen, U.R. & Aubert, J., 2006. Scaling properties of convection-driven dynamos in rotating spherical shells and application to planetary magnetic fields, *Geophys. J. Int.,* **166,** 97–114.

Cox, C.M. & Chao, B.F., 2002. Detection of large-scale mass redistribution in the terrestrial system since 1998, *Science,* **297,** 831–833.

Cox, C.M., Au, A., Boy, J.-P. & Chao, B.F., 2004. Time-variable gravity: using satellite-laser-ranging as a tool for observing long term changes in the Earth system, in *Proceedings from the 13th International Workshop on Laser Ranging*, eds Noomen, R., Klosko, S., Noll, C. & Pearlman, M., NASA/CP-2003-212248.

Dai, W. & Song, X., 2008. Detection of motion and heterogeneity in Earth's liquid outer core, *Geophys. Res. Lett.,* **35,** L16311, doi:10.1029/2008GL034895.

Defraigne, P., Dehant, V. & Wahr, J.M., 1996. Internal loading of an inhomogeneous compressible Earth with phase boundaries, *Geophys. J. Int.,* **125,** 173–192.

Dormy, E., Soward, A.M., Jones, C.A., Jault, D. & Cardin, 2004. The onset of thermal convection in rotating spherical shells, *J. Fluid Mech.,* **501,** 43–70.

Dumberry, M., 2008. Decadal variations in gravity caused by a tilt of the inner core, *Geophys. J. Int.,* **172,** 921–933.

Dumberry, M. & Bloxham, J., 2004. Variations in the Earth's gravitational field caused by torsional oscillations in the core, *Geophys. J. Int.,* **159,** 417–434.

Dumberry, M. & Bloxham, J., 2006. Azimuthal flows in the Earth's core and changes in length of day at millennial timescales, *Geophys. J. Int.,* **165,** 32–46.

Eymin, C. & Hulot, G., 2005. On core surface flows inferred from satellite magnetic data, *Phys. Earth planet. Inter.,* **152,** 200–220.

Fang, M., Hager, B.H. & Herring, T.A., 1996. Surface deformation caused by pressure changes in the fluid core, *Geophys. Res. Lett.,* **23,** 1493–1496.

Gillet, N. & Jones, C.A., 2006. The quasi-geostrophic model for rapidly rotating spherical convection outside the tangent cylinder, *J. Fluid Mech.,* **554,** 343–369.

Gillet, N., Pais, A. & Jault, D., 2009. Ensemble inversion of time-dependent core flow models, *Geochem. Geophys. Geosyst.,* **10,** Q06004, doi:10.1029/2008GC002290.

Gire, C. & Le Mouël, J.-L., 1990. Tangentially geostrophic flow at the core-mantle boundary compatible with the observed geomagnetic secular variation: the large-scale component of the flow, *Phys. Earth planet. Inter.,* **59,** 259–287.

Greff-Lefftz, M. & Legros, H., 1995. Core mantle coupling and polar motion, *Phys. Earth planet. Inter.,* **91,** 273–283.

Greff-Lefftz, M. & Legros, H., 2007. Fluid core dynamics and degree-one deformations: Slichter mode and geocenter motions, *Phys. Earth planet. Inter.,* **161,** 150–160.

Greff-Lefftz, M., Pais, M.A. & LeMouël, J.-L., 2004. Surface gravitational field and topography changes induced by the Earth's fluid core motions, *J. Geod.,* **78,** 386–392.

Gubbins, D. & Roberts, P.H., 1987. Magnetohydrodynamics of the Earth's core, in *Geomagnetism*,Vol. 2, pp. 1–184, ed. Jacobs, J.A., Academic Press, London.

Hager, B.H., Clayton, R.W., Richards, M.A., Comer, R.P. & Dziewonski, A., 1985. Lower mantle heterogeneity, dynamic topography and the geoid, *Nature,* **313,** 541–545.

Hager, B.H., Clayton, R.W. & Richards, M.A., 1989. Long-wavelength variations in Earth's geoid: physical models and dynamical implications, *Phil. Trans. R. Soc. Lond., A,* **328,** 309–327.

Hide, R., Boggs, D.H., Dickey, J.O., Dong, D., Gross, R.S. & Jackson, A., 1996. Topographic core-mantle coupling and polar motion on decadal time-scales, *Geophys. J. Int.,* **125,** 599–607.

Hills, R.G., 1979. Convection in the Earth's mantle due to viscous shear at the core-mantle interface and due to large-scale buoyancy, *PhD thesis*, N.M. State Univ., Las Cruces.

Hinderer, J., Gire, C., Legros, H. & Le Mouël, J.-L., 1987. Geomagnetic secular variation, core motions and implications for the Earth's wobble, *Phys. Earth planet. Inter.,* **49,** 121–132.

Hinderer, J., Legros, H., Jault, D. & Le Mouël, J.-L., 1990. Core-mantle topographic torque: a spherical harmonic approach and implications for the excitation of the Earth's rotation by core motions, *Phys. Earth planet. Inter.,* **59,** 329–341.

Hinderer, J., Crossley, D. & Warburton, R.J., 2007. Gravimetric methods—superconducting gravity meters, in *Treatise on Geophysics*,Vol. 3, Chap. 4, pp. 65–122, eds Schubert, G. & Herring, T., Elsevier, Amsterdam.

Holme, R., 2007. Large-scale flow in the core, in *Treatise on Geophysics*,Vol. 8, Chap. 4, pp. 107–130, eds Schubert, G. & Olson, P., Elsevier, Amsterdam.

Hulot, G., Le Mouël, J.-L. & Jault, D., 1990. The flow at the core-mantle boundary: symmetry properties, *J. Geomag. Geoelectr.,* **42,** 857–874.

Hulot, G., Le Huy, M. & Le Mouël, J.-L., 1996. Influence of core flows on the decade variations of the polar motion, *Geophys. Atrophys. Fluid Dyn.,* **82,** 35–67.

Jackson, A. & Bloxham, J., 1991. Mapping the fluid flow and shear near the core surface using the radial and horizontal components of the magnetic field, *Geophys. J. Int.,* **105,** 199–212.

Jackson, A., Bloxham, J. & Gubbins, D., 1993. Time-dependent flow at the core surface and conservation of angular momentum in the coupled core-mantle system, in *Dynamics of the Earth's Deep Interior and Earth Rotation*,Vol. 72, pp. 97–107, eds Le Mouël, J.-L., Smylie, D.E. & Herring, T., AGU Geophysical Monograph, Washington, DC.

Jackson, A., Jonkers, A.R.T. & Walker, M.R., 2000. Four centuries of geomagnetic secular variation from historical records, *Phil. Trans. R. Soc. Lond., A,* **358,** 957–990.

Jault, D., 2008. Axial invariance of rapidly varying diffusionless motions in the Earth's core interior, *Phys. Earth planet. Inter.,* **166,** 67–76.

Jault, D. & Le Mouël, J.-L., 1991. Physical properties at the top of the core and core surface motions, *Phys. Earth planet. Inter.,* **68,** 76–84.

Jault, D., Gire, C. & Le Mouël, J.-L., 1988. Westward drift, core motions and exchanges of angular momentum between core and mantle, *Nature,* **333,** 353–356.

Jiang, W., Kuang, W., Chao, B., Fang, M. & Cox, C., 2007. Understanding time-variable gravity due to core dynamical processes with numerical geodynamo modeling, in *Dynamic Planet*, Vol. 130: International Association of Geodesy Symposia, pp. 473–479, Springer, Berlin Heidelberg.

Kaula, W.M., 1968. *An Introduction to Planetary Physics*, John Wiley & Sons, Inc., New York.

Kohler, M.D. & Stevenson, D.J., 1990. Modeling core fluid motions and the drift of magnetic field patterns at the cmb by use of topography obtained by seismic inversion, *Geophys. Res. Lett.,* **17,** 1473–1476.

Lay, T., Hernlund, J. & Buffett, B.A., 2008. Core-mantle boundary heat flow, *Nat. Geosci.,* **1,** 25–32.

Le Mouël, J.-L., 1984. Outer core geostrophic flow and secular variation of Earth's magnetic field, *Nature,* **311,** 734–735.

Merriam, J.B., 1988. Limits on lateral pressure gradients in the outer core from geodetic observations, *Phys. Earth planet. Inter.,* **50,** 280–290.

Mitrovica, J.X. & Peltier, W.R., 1993. Present-day variations in the zonal harmonics of the Earth's geopotential, *J. geophys. Res.,* **98,** 4509–4526.

Mound, J.E. & Buffett, B.A., 2003. Interannual oscillations in the length of day: implications for the structure of mantle and core, *J. geophys. Res.,* **108**(B7), 2334, doi:10.1029/2002JB002054.

Olson, P., Christensen, U.R. & Glatzmaier, G.A., 1999. Numerical modeling of the geodynamo: mechanisms of field generation and equilibration, *J. geophys. Res.,* **104,** 10 383–10 404.

Pais, M.A. & Jault, D., 2008. Quasi-geostrophic flows responsible for the secular variation of the Earth's magnetic field, *Geophys. J. Int.,* **173,** 421–443.

Peltier, W.R. & Jiang, X., 1996. Glacial isostatic adjustment and Earth rotation: refined constraints on the viscosity of the deepest mantle, *J. geophys. Res.,* **101,** 3269–3290.

Richards, M.A. & Hager, B.H., 1984. Geoid anomalies in a dynamic Earth, *J. geophys. Res.,* **89,** 5987–6002.

Roberts, P.H. & Scott, S., 1965. On the analysis of secular variation, *J. Geomag. Geoelectr.,* **17,** 137–151.

Rubincam, D.P., 1984. Postglacial rebound observed by LAGEOS and the effective viscosity of the lower mantle, *J. geophys. Res.,* **89,** 1077–1087.

Sabaka, T.J., Olsen, N. & Purucker, M.E., 2004. Extending comprehensive models of the Earth's magnetic field with ørsted and CHAMP data, *Geophys. J. Int.,* **159,** 521–547.

Steinberger, B. & O'Connell, R.J., 1997. Changes of the Earth's rotation axis owing to advection of mantle density heterogeneities, *Nature,* **387,** 169–173.

Stevenson, D.J., 1987. Limits on lateral density and velocity variations in the Earth's core, *Geophys. J. R. astr. Soc.,* **88,** 311–319.

Tamisiea, M.E., Mitrovica, J.X. & Davis, J.L., 2007. GRACE gravity data constrain ancient ice geometries and continental dynamics over Laurentia, *Science,* **316,** 881–883.

Tapley, B.D., Bettadpur, M., Watkins, M. & Reigber, C., 2004. The gravity recovery and climate experiment: mission overview and early results, *Geophys. Res. Lett.,* **31,** L09607, doi:10.1029/2004GL019920.

Whaler, K.A., 1980. Does the whole of the Earth's core convect, *Nature,* **287,** 528–530.

Whaler, K.A. & Davis, R.G., 1997. Probing the Earth's core with geomagnetism, in *Earth's Deep Interior, the Doornbos Memorial Volume*, pp. 114–166, ed. Crossley, D., Gordon and Breach Science Publishers, Amsterdam.

Yoder, C.F., Williams, J.G., Dickey, J.O., Schutz, B.E., Eanes, R.J. & Tapley, B.D., 1983. Secular variation of the Earth's gravitational harmonic J_2 coefficient from LAGEOS and nontidal acceleration of Earth rotation, *Nature,* **303,** 757–762.

APPENDIX A: ELASTIC CONTRIBUTION TO THE GRAVITATIONAL POTENTIAL AT THE SURFACE

In this appendix, we describe how the parameters $\kappa_l(r)$ are calculated. These characterize the elastic response of the Earth to a density perturbation $\rho'(r)$ concentrated in a thin radial surface of thickness $\mathrm{d}r$ at radius r in the fluid outer core. Accordingly, we express this density perturbation in terms of a surface mass density $\sigma(r) = \rho'(r)\,\mathrm{d}r$ and, following the notation introduced in the main text, $\sigma_\alpha(r)$ is used to denote a single spherical harmonic coefficient of $\sigma(r)$.

The perturbation in gravitational potential at the surface, $\phi_\alpha \equiv \phi_\alpha(r_e)$, due to the presence of $\sigma_\alpha(r_1)$ at a specific radius r_1 in the fluid core is comprised of two parts: that from the density perturbation,

$$\phi_\alpha^{(1)} = -\frac{4\pi G}{2l+1}\frac{r_1^{l+2}}{r_e^{l+1}}\sigma_\alpha(r_1)\,, \tag{A1}$$

and a part denoted by $\phi_\alpha^{(2)}$ from the density variations that result from global elastic deformations in response to the presence of $\sigma_\alpha(r_1)$. For small perturbations, $\phi_\alpha^{(2)}$ is linearly related to $\phi_\alpha^{(1)}$ and we express this relationship by

$$\phi_\alpha^{(2)} = \kappa_l(r_1)\,\phi_\alpha^{(1)}\,, \tag{A2}$$

such that

$$\phi_\alpha = \phi_\alpha^{(1)}\,[1 + \kappa_l(r_1)]\,. \tag{A3}$$

The procedure to find the parameters $\kappa_l(r_1)$ is very similar to that described in Dumberry & Bloxham (2004, hereinafter referred to as DB), and where further references to the literature can be found. For brevity, the procedure is not repeated in detail here. Instead, we refer the reader to the equations and notation given in DB, and point out the important modifications.

The presence of $\sigma_\alpha(r_1)$ represents a forcing that perturbs the global hydrostatic equilibrium between stress and gravity. This forcing leads to small displacements which, in turn, perturb the stress and gravity field. A new mechanical equilibrium is reached, in which the forcing is balanced by the sum of the forces induced by the small displacements. To find this new equilibrium, we must solve the momentum equation jointly with Poisson's equation. The combined equations can be written as a set of elasto-gravitational equations.

Perturbations in the mantle and inner core must satisfy the set of elasto-gravitational equations given, respectively, by eqs (14) and (18) of DB but with no externally applied body force (i.e. $\mathbf{f} = \mathbf{f}^s = \mathbf{0}$). Perturbations in the fluid core, when hydrostatic equilibrium is assumed to be maintained in the deformed state and deformations are assumed divergence-free, are simpler than those in the solid Earth: only Poisson's equation must be solve and the deformed surfaces of constant gravitational potential, density and pressure remain in alignment. This is expressed by eq. (30) of DB.

The forcing from $\sigma_\alpha(r_1)$ is introduced by imposing continuity of the gravitational potential and gravitational flux at the radial surface r_1. In the notation of DB, these conditions are expressed by

$$y_5(r_1^+) = y_5(r_1^-)\,, \tag{A4}$$

$$y_6(r_1^+) = y_6(r_1^-) + 4\pi G\sigma_\alpha\,, \tag{A5}$$

where G is the gravitational constant and the superscripts '+' and '−' refer to quantities evaluated above and below r_1, respectively. This procedure follows that which is used to model elastic deformations caused by density heterogeneities in the mantle (e.g. Defraigne *et al.* 1996). We note that, unlike in the mantle, additional boundary conditions on displacement and stress are not required at r_1; hydrostatic equilibrium is assumed to be maintained in the deformed state, in which case the (Eulerian) displacement of the equipotential surfaces and change in (Eulerian) pressure are simply related to the change in gravitational potential (eqs 24 and 25 of DB, with $p_g = 0$).

The mechanical equilibrium of the deformed state in the whole Earth is then solved by integrating the elasto-gravitational equations from a small radius to the surface, propagating the solution across each interface, including r_1, according to specified boundary conditions. The boundary conditions at $r \to 0$ are given by eq. (45) of DB; the boundary conditions at the ICB are given by eqs (42)–(44) of DB [with $\Psi_n^0(c) = 0$]; those at the CMB are given by eq. (41) of DB [with $\Psi_n^0(b) = 0$]; at the surface, the conditions in eq. (46) of DB are employed.

The perturbation in gravitational potential at the surface from this procedure, denoted by $y_5(r_e)$, represents the total perturbation, the sum of $\phi_\alpha^{(1)}$ and $\phi_\alpha^{(2)}$. The value of $\kappa_l(r_1)$ at a spherical harmonic degree l is then given by

$$\kappa_l(r_1) = -1 + \frac{y_5(r_e)}{\phi_\alpha^{(1)}}\,. \tag{B6}$$

The procedure is repeated for different values of r_1 between the ICB and the CMB.